Leveling the Mountain Range of Excited-State Benchmarking through Multistate Density Functional Theory

Hong Zhu,[1,2] Ruoqi Zhao,[2] Meiyi Liu,[2*] Jun Zhang,[2*] and Jiali Gao[1,2,3*]

[1] *School of Chemical Biology & Biotechnology, Peking University Shenzhen Graduate School, Shenzhen, Guangdong 518055, China*

[2] *Institute of Systems and Physical Biology, Shenzhen Bay Laboratory, Shenzhen Guangdong 518055, China*

[3] *Department of Chemistry and Supercomputing Institute, University of Minnesota, Minneapolis, Minnesota 55455, USA*

* Corresponding authors: e-mails: liumy@szbl.ac.cn (ML), zhangjun@szbl.ac.cn, (JZ), and gao@jialigao.org (JG).

Key words: Multistate density functional theory, transition density functional, excited states, density functional theory, MSDFT.

Abstract: The performance of multistate density functional theory (MSDFT) with nonorthogonal state interaction (NOSI) is assessed for 100 vertical excitation energies against the theoretical best estimates (TBE) extracted to the full configuration interaction accuracy on the database developed by Loos, P.F., at al. in 2018 (Loos2018). Two optimization techniques, namely block-localized excitation (BLE) and target state optimization (TSO), are examined along with two ways of estimating the transition density functional (TDF) for the correlation energy of the Hamiltonian matrix density functional. The results from the two optimization methods are similar. It was found that MSDFT-NOSI using the spin-multiplet degeneracy (SMD) constraint for the TDF of spin-coupling interaction, along with the M06-2X functional, yields a root-mean-square error (RMSE) of 0.22 eV, better than CIS(D_∞), CC2, and ADC(3) all of which have an RMSE of 0.28 eV, but somewhat less than STEOM-CCSD (RMSE of 0.14 eV) and CCSD (RMSE of 0.11 eV) wave function methods. Interestingly, MSDFT-NOSI performs noticeably better than TDDFT at an RMSE of 0.43 eV using the same functional and basis set on the Loos2018 database. In comparison with the ground state and the lowest triplet energies from KS-DFT calculations, it was found that the multistate DFT approach has little double counting of correlation. Importantly, there is no noticeable difference in the performance of MSDFT-NOSI on valence, Rydberg, singlet, triplet, and double-excitation states. Although the use of another hybrid functional PBE0 leads to a greater RMSE of 0.36 eV, the deviation is systematic with a linear regression slope of 0.994 against the results with M06-2X. The present benchmark reveals that density functional approximations developed for KS-DFT for the ground state with a non-interacting reference may be adopted in MSDFT calculations in which state interaction is key.

1. Introduction

The Gaussian-n series of benchmarks of electronic structure calculations set a standard for modern model chemistry,[1-4] which stimulated such investigations like bamboo shoots after a spring rain. Benchmark studies are both critical and valuable for evaluating the performance of a theoretical model and for designing new methods to further improve its accuracy.[5, 6] Numerous investigations have been reported, including ground-state and excitation energies; however, it is the latter that is especially challenging because both static and dynamic correlation are often necessary to achieve adequate accuracy.[5-12] In a series of recent studies of excitation energies of molecular systems using wave function theory (WFT), Loos and coworkers likened the effort as mountaineering through the ever-ascending peaks of theoretical models.[13-17] These systematic approaches helped establish theoretical best estimates (TBE) of vertical transition energies that can be used to evaluate the performance of more efficient methods.[5, 17] Benchmarking Kohn-Sham density functional theory (KS-DFT)[18] on relative ground-state energies and linear-response time-dependent DFT (TDDFT) on excitation energies has also been popular,[19-25] but they are almost exclusively limited to examining density functional approximations. The systematic strategy of mountaineering excited states in WFT was not possible in KS-DFT based on the theorems of Hohenberg and Kohn (HK) for the ground state.[26] To this end, Lu and Gao in 2021 established the fundamental principles of DFT for all states,[27] proving the existence of a Hamiltonian matrix density functional (HMDF) $\boldsymbol{\mathcal{H}}[\boldsymbol{D}(\boldsymbol{r})]$ for any number of the lowest N eigenstates.[28] The multistate density functional theory (MSDFT) offers opportunities to develop novel density functional approximations beyond the realm of traditional HKS-DFT and to treat both the ground state and excited states on an equal footing.[29] By introducing a minimal active space (MAS) according to the theorem of Lu and Gao,[30-32] we can retain the original benefits of

DFT with a balanced treatment of computational efficiency and accuracy in light of increased complexity of multiple states. In this article, we present the results from a nonorthogonal state interaction (NOSI) method in the framework of MSDFT.[28, 33] The findings are compared with the TBE of WFT on a list of benchmark molecules that has been established previously.[13]

A wide range of benchmark sets of excitation energies have been developed in the past (for a rather comprehensive list of studies, see references [12] and [25]), of which the comprehensive study of twenty-eight small molecules by Thiel and coworkers in 2008 was the most representative.[5] Recently, Loos et al. created a set of accurate excitation energies for eighteen small molecules,[13] having considered several factors that balance accurate molecular geometries and basis sets with diffuse functions, treatment of electron correlation using coupled cluster theory (CC) and selected configuration interaction (sCI), and vertical excitation and fluorescence energies. The accuracy of the transition energies of this dataset is close to the full CI (FCI) quality by systematically increasing the order of the CC expansion and determinant selection in sCI, coupled with basis set extrapolation to the complete basis set limit. Aiming for different purposes, the authors created two sets of TBE of excitation energies by using extracted FCI (exFCI) with the aug-cc-pVTZ basis set and by including all electron contributions and basis set extrapolation.[13] Of the two sets of TBE, the difference between frozen core approximation and full electron treatment of correlation is rather small, within 0.01-0.02 eV, while greater effects are mainly from basis sets. Nevertheless, the two sets of TBE are not very different, typically within 0.05 eV in excitation energies. Then, a list of 12 different methods in WFT were assessed against the TBE/aug-cc-pVTZ results, revealing that the best performance is found in CCSDT and CCSDTQ methods with a root-means-square error (RMSE) of 0.03 and 0.02 eV, respectively, and the CIS(D), ADC(2) and ADC(3) methods have somewhat larger deviations with average errors of about 0.3 eV.[13] One particularly attractive

feature, in addition to a more systematic and accurate benchmark than prior studies, is to have a set of well-defined vertical transition energies from theory without the complication of extracting from experimental uncertainties. Consequently, this list of compounds is adopted to assess the performance of multistate DFT.

Density functional theory based on the Hohenberg-Kohn-Sham method is an indispensable tool in modern computational chemistry for large systems. Nevertheless, it is a ground-state theory without a clear path for designing density functional approximations for the rest of the solutions of the Schrödinger equation.[34] Although TDDFT can be used to determine excitation energies, giving excellent results for many molecules, it is based on response approaches fundamentally rooted in the ground of HKS-DFT and its shortcomings are well documented.[25, 35] For electronic excited state, Theophilou showed that the subspace spanned by the lowest two states of a system is solely determined by the sum of their electron densities, called subspace density $\rho_V(\boldsymbol{r}) = [\rho_1(\boldsymbol{r}) + \rho_2(\boldsymbol{r})]/2$, from which the sum of the eigenstate energies is also determined.[36] However, Theophilou's subspace theory does not directly give the energies and densities of the individual states, rendering the method to have little use in the literature. Re-formulation of the subspace theory with the introduction of weights over different states[37, 38] still fundamentally cannot escape from the need for knowing the subspace energies of all lower orders to obtain the excitation energy of a given excited state, *i.e.*, a gradual build-up approach. The origin of this problem lies in the choice of the fundamental variable required to determine each individual eigenstate E_I $(I = 1, \cdots, N)$.[36, 39] It is the multistate matrix density $\boldsymbol{D}(\boldsymbol{r})$ that is necessary and sufficient to resolve the individual eigenstates,[39] whereas the subspace density $\rho_V(\boldsymbol{r})$ alone, although sufficient for the sum (or weighted sum) of *N*-states,[36] contains insufficient information to distinguish individual states.[39] The implication of this requirement is that state interaction is necessary in DFT to treat

excited states without relying on a response theory,[40] a conceptual difference from the non-interacting device in KS-DFT for one state.[18] The good news, however, is that unlike WFT, a minimal active space (MAS) exists, keeping the spirit of computational efficiency, to exactly represent the fundamental variable $\boldsymbol{D}(\boldsymbol{r})$.[28, 39]

In the following, we first present the fundamental theory of MSDFT and the computational procedure of NOSI. Then, we illustrate the MSDFT-NOSI method against the best theoretical estimates from the work of Loos, et al.,[13] making use of two popular density functional approximations developed for the KS-DFT, namely the Minnesota M06-2X and the hybrid PBE0 models.[41-44] We also compare the performance of TDDFT that works well for many compounds.[25] It is hoped that the present assessment, along with the previous evaluations of organic compounds and exciplex complexes against TDDFT,[32, 45] of local valence and charge transfer excitations against EOM-CCSDT,[30] and of core-level excitations of open-shell species[46] shall stimulate further developments of multistate models in density functional theory and design of transition density functional approximations for excited states.

2. Theory

In this section, we first summarize the fundamentals of multistate density functional theory, followed by introduction of a minimal active space to represent the multistate matrix density and a correlation matrix functional. Then, we describe the computational method of nonorthogonal state interaction (NOSI) used in the present study.

A. Multistate Density Functional Theory. MSDFT[33, 40] is based on three fundamental theorems[29] that establish (i) the existence of a Hamiltonian matrix density functional (HMDF) for the lowest N eigenstates, (ii) a variational principle for multistate optimization to yield exactly the energies and densities of all N states, and (iii) the representation of the N-dimensional matrix (N-

matrix) density $\boldsymbol{D}(\boldsymbol{r})$ by no more than N^2 Slater determinants. For a molecular system described by the Hamiltonian $\hat{H} = \hat{H}^o + v_{ext}(\boldsymbol{r})$, where $\hat{H}^o$ consists of kinetic and electronic repulsion operators and $v_{ext}(\boldsymbol{r})$ is the local external potential, $\boldsymbol{D}(\boldsymbol{r})$ is a matrix of electron densities $\{\rho_i(\boldsymbol{r}) \equiv \rho_{ii}(\boldsymbol{r}); i = 1, \cdots, N\}$ and transition densities $\{\rho_{ij}(\boldsymbol{r}); i \neq j, i, j = 1, \cdots, N\}$.

$$\boldsymbol{D}(\boldsymbol{r}) = \begin{pmatrix} \rho_1(\boldsymbol{r}) & \cdots & \rho_{N1}(\boldsymbol{r}) \\ \vdots & \ddots & \vdots \\ \rho_{1N}(\boldsymbol{r}) & \cdots & \rho_N(\boldsymbol{r}) \end{pmatrix} \tag{1}$$

These theorems are summarized below.

i. In the subspace $\mathbb{V}$ spanned by the lowest *N* eigenstates, $\hat{H}$ is a matrix density functional (HMDF) of $\boldsymbol{D}(\boldsymbol{r})$:

$$\boldsymbol{\mathcal{H}}[\boldsymbol{D}] = \boldsymbol{\mathcal{F}}[\boldsymbol{D}] + \int \boldsymbol{D}(\boldsymbol{r}) v_{ext}(\boldsymbol{r}) d\boldsymbol{r} \tag{2}$$

where $\boldsymbol{\mathcal{F}}[\boldsymbol{D}]$ is the universal Hamiltonian matrix functional, independent of the external potential $v_{ext}(\boldsymbol{r})$. In short, theorem 1 establishes a one-to-one correspondence between $\boldsymbol{D}$ and $\boldsymbol{\mathcal{H}}$.

ii. For any *N*-matrix trial density $\boldsymbol{D}'(\boldsymbol{r})$, the multistate energy, defined as the trace of $\boldsymbol{\mathcal{H}}[\boldsymbol{D}'(\boldsymbol{r})]$, $E'_{MS}[\boldsymbol{D}'(\boldsymbol{r})] = tr\{\boldsymbol{\mathcal{H}}[\boldsymbol{D}']\}$, is greater than or equal to the multistate energy $E_{MS}[\boldsymbol{D}]$ of the subspace $\mathbb{V}$:

$$E'_{MS}[\boldsymbol{D}'(\boldsymbol{r})] \geq E_{MS}[\boldsymbol{D}(\boldsymbol{r})] \tag{3}$$

The equal sign is true if the trial density is a matrix density of the subspace $\mathbb{V}$, *i.e.*, $\boldsymbol{D}'(\boldsymbol{r}) = \boldsymbol{D}(\boldsymbol{r})$. Then, diagonalization of the Hamiltonian matrix $\boldsymbol{\mathcal{H}}[\boldsymbol{D}]$ yields exactly all *N* eigenstate energies, including the ground state and the lowest $N-1$ excited states.

iii. The multistate *N*-matrix density $\boldsymbol{D}(\boldsymbol{r})$ can be sufficiently represented by N^2 independent Slater determinant wave functions.[39]

In the special case where $N = 1$, $\boldsymbol{\mathcal{H}}[\boldsymbol{D}(\boldsymbol{r})]$ is reduced to a scalar energy density functional of the ground-state density: $\mathrm{E}_0 = E[\rho_0(\boldsymbol{r})]$, giving rise to the Hohenberg and Kohn theorem for the ground state. Then, according to Theorem 3, $\rho_0(\boldsymbol{r})$ can be represented exactly by one single Slater determinant as in KS-DFT.

The three theorems proved the existence and the structure of density functional theory for all states of the Schrödinger equation. The exact form and expression of the universal matrix functional, just as that of the Hohenberg and Kohn theorem for the ground state, is unknown, nor do the theorems tell the precise way of selecting the specific determinants for density representation. MSDFT offers ways, beyond the scope of a non-interacting reference for the ground state, to develop different methods for constructing the HDMF and optimizing $\boldsymbol{D}(\boldsymbol{r})$. In this work, we present one such computational procedure, akin to nonorthogonal configuration interaction (NOCI) in WFT. Yet, the present NOSI differs from NOCI because dynamic correlation is included in each determinant state optimization, a dynamic-then-static ansatz championed by Liu and coworkers.[47, 48] In this regard, an analogy in WFT is to introduce dynamic correlation to basis states from multiconfigurational self-consistent-field (MCSCF) calculations, followed by multistate interaction, such as MS-CASPT2 and MRCI approaches. Significantly, NOSI is constructed in an *N*-dimensional subspace that is complete, yet, has an upper bound in the number of auxiliary states in the active space to exactly represent the densities of all *N* states.

B. Minimal Active Space. The fundamental variable required to resolve the individual states of the subspace $\mathbb{V}$ is the multistate *N*-matrix density $\boldsymbol{D}(\boldsymbol{r})$.[39] Therefore, representation of the *N*-matrix density is of central importance in a density functional theory for multiple states. However, density representation is not unique. Consequently, different computational methods can be designed. According to Theorem 3 of Lu and Gao, $\boldsymbol{D}(\boldsymbol{r})$ can be exactly represented by no more

than N^2 Slater determinants.[28, 39] In this case, molecular orbitals for different Slater determinants are generally nonorthogonal. Lu and Gao also showed that it is possible to employ a common set of orthogonal orbitals to exactly represent $\boldsymbol{D}(\boldsymbol{r})$, and an SCF approach for an active space consisting of singly and doubly excited configurational states was introduced.[39] In either scenario, it should be kept in mind that there is an upper bound in the number of configurations to exactly represent $\boldsymbol{D}(\boldsymbol{r})$, and there is no need to use more determinants than necessary.[39] Obviously, this concept is different from multiconfigurational methods in WFT.

In this work, we use a minimal active space (MAS) representation, keeping the spirit of computational efficiency of DFT, for the excited states featured in the Loos2018 dataset. Although the *N*-matrix density $\boldsymbol{D}(\boldsymbol{r})$ could be directly optimized using N^2 Slater determinants, here, we take an alternative route by constructing a set of *N* auxiliary multistate wavefunctions $\{\Phi_A; A = 1, \cdots, N\}$ for representing $\boldsymbol{D}(\boldsymbol{r})$. The auxiliary wave functions are expressed as a linear combination of Slater determinants in the MAS, $V_{MAS} = \{\Xi_\xi; \xi = 1, \cdots, M\}$ with $M \sim N^2$.[29-31]

$$\Phi_A = \sum_{\xi}^{M} c_{\xi A}\, \Xi_\xi \tag{4}$$

where Ξ_ξ is the ξth Slater determinant, constructed from n_e (the number of electrons) one-body spin orbitals $\{\psi_{i\sigma}^{\xi}\}$, and $c_{\xi A}$ is a configuration coefficient for auxiliary state *A*.

$$\Xi_\xi(r_1, \cdots, r_{n_e}) = \frac{1}{\sqrt{n_e!}} \hat{A}\{\psi_{1\sigma_1}^{\xi}(r_1) \cdots \psi_{n_e\sigma_{n_e}}^{\xi}(r_{n_e})\} \tag{5}$$

In general, the orbitals of the same determinant are orthonormal, $< \psi_{i\sigma_i}^{\xi} | \psi_{j\sigma_j}^{\xi} > = \delta_{ij}\delta_{\sigma_i\sigma_j}$, but they are nonorthogonal from different determinants. Of course, each molecular orbital is expressed as a linear combination of atomic basis orbitals. Consequently, the optimization of the multistate

N-matrix density $\boldsymbol{D}(\boldsymbol{r})$ is equivalently transformed to the optimization of orbital and configuration coefficients.

The lowest *N* eigenstates of the Hamiltonian matrix functional in terms of the determinant basis configurations of the MAS (see below) are chosen as the auxiliary basis states of the subspace $\mathbb{V}$, noticing that the total number of degrees of freedom used to optimize $\boldsymbol{D}(\boldsymbol{r})$, given either in the determinant basis or in the auxiliary wave function basis, remains unchanged. Then, each element of the multistate *N*-matrix density is obtained as follows.

$$D_{AB}(r) =< \Phi_A(r)|\hat{\rho}|\Phi_B(r) > \tag{6}$$

where $\hat{\rho}$ is the density operator.

C. Correlation Matrix Functional. Given the minimal active space V_{MAS} that is used to exactly represent $\boldsymbol{D}(\boldsymbol{r})$ of the *N*-dimensional subspace $\mathbb{V}$ via the auxiliary states $\{\Phi_A; A = 1, \cdots, N\}$, the correlation matrix functional is defined as the difference between the universal matrix functional $\boldsymbol{\mathcal{F}}[\boldsymbol{D}]$ and the multistate kinetic and Hartree-exchange terms from one-body orbitals:

$$\boldsymbol{\mathcal{E}}_c[\boldsymbol{D}(\boldsymbol{r})] = \boldsymbol{\mathcal{F}}[\boldsymbol{D}(\boldsymbol{r})] - (\boldsymbol{T}_{ms} + \boldsymbol{E}_{Hx}) \tag{7}$$

where the elements of the last two terms are determined using the auxiliary wave functions by

$$< \Phi_A|\hat{H}^o|\Phi_B > = (\boldsymbol{T}_{ms})_{AB} + (\boldsymbol{E}_{Hx})_{AB} \tag{8}$$

The physical interpretation of the correlation matrix functional (eq 7) is that it represents the remaining correlation energy of the multistate energy of the subspace $\mathbb{V}$ that is not explicitly included in the auxiliary wave functions (which is used to represent exactly $\boldsymbol{D}(\boldsymbol{r})$).[28, 40]

Computationally, it is more convenient to express the total Hamiltonian and correlation matrix functionals in terms of the determinant configurations in V_{MAS} (via the coefficient matrix in eq 4). Then, the Hamiltonian matrix density functional is written as follows.

$$H_{\xi\eta}[\boldsymbol{D}] = (T_{ms})_{\xi\eta} + (E_{Hx})_{\xi\eta} + \int d\boldsymbol{r} D_{\xi\eta}(\boldsymbol{r}) v_{ext}(\boldsymbol{r}) + (E_c[\boldsymbol{D}])_{\xi\eta} \tag{9}$$

where ξ and η are indices of the determinants in V_{MAS}, and the notation $(E_c[\boldsymbol{D}])_{\xi\eta}$ emphasizes that the matrix element $(E_c)_{\xi\eta}$ is generally dependent on the full matrix density function $\boldsymbol{D}(\boldsymbol{r})$, rather than a term-by-term mapping $(E_c[D_{\xi\eta}])_{\xi\eta}$.[29] Clearly, the first three terms of eq 9 can be directly obtained from the one-body orbitals of the nonorthogonal determinant states.[49-51] Then, eq 9 can be simplified as follows.

$$H_{\xi\eta}[\boldsymbol{D}] = < \Xi_\xi \left| \widehat{H} \right| \Xi_\eta > + (E_c[\boldsymbol{D}])_{\xi\eta} \tag{10}$$

It is important to point out that since the diagonal matrix elements $(E_c)_{\xi\xi}$ are given in terms of determinant configurations, it suggests that these terms may be approximated by using the exchange-correlation functionals developed in the framework of KS-DFT.

D. Nonorthogonal State Interaction. In this work, we adopt nonorthogonal state interaction (NOSI) in multistate density functional theory to determine the ground and excited state energies. The method consists of two computational steps.[29]

First, we independently optimize the ground-state and excited-state determinants, Ξ_ξ ($\xi = 1, \cdots, M$). Note that the number of determinants M in the MAS is not always precisely restricted to N^2, depending on the inclusion of all spin complement determinants and the adiabatic states of interest. An important task in this step is to keep a given non-aufbau occupation unchanged in the optimization process, and we have developed two approaches to accomplish this goal.[52-54] In the block-localized excitation (BLE) method,[52] we use a ground-state orbital projection to retain the order of orbitals in the non-aufbau configuration, $\left(\boldsymbol{T}_0^\dagger \boldsymbol{F} \boldsymbol{T}_0\right)\boldsymbol{T} = \left(\boldsymbol{T}_0^\dagger \boldsymbol{S} \boldsymbol{T}_0\right)\boldsymbol{T}\boldsymbol{\epsilon}^{\mathrm{BLE}}$, where $\boldsymbol{T}_0$ and $\boldsymbol{T}$ are the orbital coefficients of the ground-state and the non-aufbau state. Thus, in each SCF iteration, the orbitals are expressed in the same order in terms of the MO basis of the ground state. Alternatively, in the target state optimization (TSO) approach,[53, 54] we first place the un-occupied molecular orbitals of the ground state below the orbital(s) of the excited electron(s) into an

auxiliary block, and then, the optimization of the non-aufbau configuration is carried out in the basis without the MOs in the auxiliary space, effectively becoming an SCF procedure for an orbital-constrained optimization. The difference between the BLE and TSO methods is that BLE is a fully variational ΔSCF procedure, but TSO is a constrained approach lacking the degrees of freedom of the auxiliary space. As a result, the energy from the TSO optimization is slightly higher than that from the BLE method. The advantage, however, is that TSO is essentially a ground-state optimization procedure without the possibility of collapsing to lower energy states. For the present case, we found that both methods are highly robust without collapsing to lower states.

In step 2 of NOSI, we obtain the energies and wave functions (densities) (eq 4) of the individual adiabatic states by minimizing the multistate energy $E_{MS} = tr\{\boldsymbol{\mathcal{H}}[\boldsymbol{D}]\}$ through a single diagonalization of the HMDF:[33]

$$E_I[\boldsymbol{D}] = \sum_{\xi}^{M} c_{\xi I}^2 \, H_{\xi\xi} + \frac{1}{2}\sum_{\xi}^{M}\sum_{\eta}^{M} c_{\xi I}\, c_{\eta I} H_{\xi\eta} \tag{11}$$

Clearly, the key is to determine the matrix elements of the HMDF $\boldsymbol{\mathcal{H}}[\boldsymbol{D}]$. As above, the diagonal terms are simply the KS-DFT energies evaluated in the optimization process of the Slater determinants in V_{MAS},[52-54] keeping in mind that the corresponding KS-determinants are non-aufbau occupation constrained.

$$\mathcal{H}_{\xi\xi} = E_{\xi}^{KS}[\rho_{\xi}(\boldsymbol{r})] \tag{12}$$

For the off-diagonal elements (eq 10), the correlation energy $(\mathcal{E}_c)_{\xi\eta}$ is called transition density functional (TDF),[40] which does not exist in HKS-DFT. Thus, further approximation is needed. Interestingly, in special situations such as spin coupling interactions between spin-mixed determinants that yield a pair of singlet and triplet ($M_s = 0$) states, $(\mathcal{E}_c)_{\xi\eta}$ can be obtained rigorously by enforcing the energy degeneracy among the high and low M_s projections of the

triplet states.[46, 55-57] Since the energy for the $M_s = 1$ triplet state of a molecule can be determined exactly (in principle) by HKS-DFT with one determinant, the TDF energy between two spin-mixed determinants $\Xi_{\xi}^{\uparrow\downarrow}$ and $\Xi_{\eta}^{\downarrow\uparrow}$ to yield the same energy for the $M_s = 0$ triplet state is uniquely determined by the TDF energy

$$(\mathcal{E}_c)_{\xi\eta}^{sp} = E_{xc}^{KS}\left[\rho_{\xi_T}^{\uparrow\uparrow}(\boldsymbol{r})\right] - E_{xc}^{KS}\left[\rho_{\xi\xi}^{\uparrow\downarrow}(\boldsymbol{r})\right] \tag{13}$$

where $E_{xc}^{KS}\left[\rho_{\xi_T}^{\uparrow\uparrow}(\boldsymbol{r})\right]$ is the "Kohn-Sham" correlation energy with the electron density $\rho_{\xi_T}^{\uparrow\uparrow}(\boldsymbol{r})$ of the spin-up triplet state $\Xi_{\xi_T}^{\uparrow\uparrow} = |\psi_{1\alpha}^{\xi}\psi_{1\beta}^{\xi}\cdots\psi_{\left(\frac{1}{2}n_e-1\right)\beta}^{\xi}\psi_{i\alpha}^{\xi}\psi_{j\alpha}^{\xi}>$, and $E_{xc}^{KS}\left[\rho_{\xi\xi}^{\uparrow\downarrow}(\boldsymbol{r})\right]$ is the KS correlation energy using $\rho_{\xi\xi}^{\uparrow\downarrow}(\boldsymbol{r})$ (equivalently with $\rho_{\eta\eta}^{\downarrow\uparrow}$) corresponding to the spin-mixed determinant state $\Xi_{\xi\xi}^{\uparrow\downarrow} = |\psi_{1\alpha}^{\xi}\psi_{1\beta}^{\xi}\cdots\psi_{\left(\frac{1}{2}n_e-1\right)\beta}^{\xi}\psi_{i\alpha}^{\xi}\psi_{j\beta}^{\xi}>$ ($\Xi_{\eta\eta}^{\downarrow\uparrow} = |\psi_{1\alpha}^{\eta}\psi_{1\beta}^{\eta}\cdots\psi_{\left(\frac{1}{2}n_e-1\right)\beta}^{\eta}\psi_{i\beta}^{\eta}\psi_{j\alpha}^{\eta}>$). The superscript *sp* in eq 13 indicates spin-pairing interactions. The subscript ξ_T in $\rho_{\xi_T}^{\uparrow\uparrow}(\boldsymbol{r})$ is used to indicate that the determinant $\Xi_{\xi_T}^{\uparrow\uparrow}$ refers to the triplet state with respect to the two spin complement determinants $\Xi_{\xi\xi}^{\uparrow\downarrow}$ and $\Xi_{\eta\eta}^{\downarrow\uparrow}$.

For all other situations, we use the overlap-weighted average correlation energy of the two interacting states to approximate their TDF:[33]

$$(\mathcal{E}_c)_{AB} = \frac{1}{2}S_{AB}\{E_{xc}^{KS}[\rho_A(\boldsymbol{r})] + E_{xc}^{KS}[\rho_B(\boldsymbol{r})]\} \tag{14}$$

We emphasize again that each basis state represented by a single Slater determinant is variationally optimized in MSDFT-NOSI.[58] Thus, the vast toolchest of approximate density functionals developed for single-determinant KS-DFT can be employed in multistate calculations.

3. Computational Details

The geometries for eighteen small molecules in the Loos2018 dataset are taken from the original study,[13], which were optimized using CC3/aug-cc-pVTZ. In this dataset, a range of one to

six singlet or triplet excited states was determined for each molecule, producing two sets of theoretical best estimates: (a) TBE(FC)/AVTZ corresponding to a frozen-core FCI extrapolation with the aug-cc-pVTZ basis, and (b) corr-TBE that is basis-set corrected at the CC3(full) level of theory. The TBE(FC)/AVTZ, simply TBE, is used as the reference in the present study.

To benchmark the MSDFT-NOSI method, we employ two popular density functional approximations for KS-DFT to determine the energies of the diagonal matrix elements of the HMDF, including the Minnesota M06-2X[41] and the PBE0 model,[42-44] along with the aug-cc-pVTZ basis set.[59] In a few cases, some excited configurations encountered difficulties to achieve convergence using the BLE method, and a different basis set was used. In particular, for H_2S and cyclopropane, the cc-pVQZ basis was used, and aug-cc-pVDZ for $CH_3CH{=}O$, $CH_2{=}C{=}O$ and $HCONH_2$.[59] We did not further investigate and optimize the SCF procedure since the relative energies for other configurations are of similar quality in comparison with the aug-cc-pVTZ results. Thus, we do not anticipate the quality of the overall performance will be affected. We also carried out optimizations for the non-aufbau configurations using the TSO method for constructing the active space, and compared the performance of the two optimization techniques for generating basis states in NOSI calculations.

Configurational states for each molecule in the MAS consist of only singly excited configurations for a standard set of active orbitals comprising two highest occupied and two lowest unoccupied Kohn-Sham molecular orbitals (HOMO-1, HOMO, LUMO and LUMO+1), i.e., S[4e,4o]. One exception is the molecule nitrosomethane (CH_3-NO), for which the second singlet excited state (1A′) is a double-excitation state corresponding to the $(n, n \rightarrow \pi^*, \pi^*)$ transition.[13] Thus, the corresponding double excited configuration is also included in the MAS. For some molecules, it turns out that the number of electrons and orbitals in this starting point can be adjusted;

for example, only two electrons for ethylene, ketene and diazomethane are sufficient in the active space for the excited states included in the Loos2018 benchmark, whereas up to six electrons are included for molecules with degenerate or nearly degenerate orbitals. A list of the determinant configurations used for each molecule is given in Table 1, but not necessarily all configurations are required. The use of only singly excited configurations in the MAS is consistent with the findings of Loos et al., who concluded that except the nitrosomethane $1A'$ state, all excited states in their dataset show more than 80% (generally more than 90%) single-transition character from CC3 analysis.[13] Importantly, the use of a MAS for each species keeps the spirit of computational efficiency of DFT.

Table 1. The number of electrons and maximum number of determinant configurations in the minimal active space for each molecule.[a]

Molecule	N_e	M_{max}	configurations
H_2O	4	9	KS, S[4e, 4o]
H_3N	6	15	KS, S[4e, 4o], (H-2) →L, H→L+2,L+3
H_2S	4	9	KS, S[4e, 4o]
HCl	4	9	KS, S[4e, 4o]
HC≡CH	4	9	KS, S[4e, 4o]
CH_2=CH_2	2	9	KS, S[2e, 5o]
Cyclo-propene	6	7	KS, S[6e, 4o]
CH_2=O	4	17	KS, S[4e, 6o]
CH_3CH=O	4	9	KS, S[4e, 4o]
CH_2=C=O	2	9	KS, S[2e, 5o]
$HCONH_2$	6	13	KS, S[4e, 5o]
CH_2=S	4	9	KS, S[4e, 4o]
CH_2=NH	4	9	KS, S[4e, 4o]
CH_3-N=O	6	14	KS, S[4e, 5o], (H-2) →L, H→L/double
CH_2=N=N	2	9	KS, S[2e, 5o]
H_2N-CH=NH_2^+	4	9	KS, S[4e, 4o]
CO	6	25	KS, S[6e, 7o]
N_2	6	25	KS, S[6e, 7o]

a. H-2 is the HOMO-2 orbital, and L and L+n are the LUMO and LUMO+n orbital.

The MSDFT-NOSI calculations were performed using the Qbics program developed in our laboratories[60] and a separate program for energy decomposition analysis interfaced with the GAMESS-US program for electronic integrals.[61] In NOSI calculations, we used a fine grid consisting of 96 radial shells and 302 angular points. For comparison, we have also determined the excitation energies using TDDFT/M06-2X/aug-cc-pVTZ with Gaussian16.[62]

4. Results and Discussion

A. Ground-State Energies. We begin with our discussion on the computed energies for the ground state and the lowest triplet state of each molecule. Listed in Table 2 are the total energies obtained from NOSI calculations and its difference relative to that calculated using KS-DFT. Nonorthogonal state interaction is a multistate DFT method, in which the Kohn-Sham determinant state is a member of the MAS. KS-DFT itself employs a non-interacting reference system, expressed by a single Slater determinant to represent the ground-state density; in principle, all electron correlation is included. However, a multistate DFT method includes state interaction amongst the configurational states in the MAS, which introduces explicitly some static correlation. Double counting of electron correlation has been a concern in multiconfigurational DFT (MC-DFT) methods in which KS-correlation energy is added to the energy from a correlated WFT.[40, 63-65]

The theory of MSDFT is rigorous without double counting correlation[28] and the approximation of NOSI differs from all other MC-DFT models in that the total electron density from a MCSCF wave function is not directly used in KS-DFT correlation energy evaluation.[33, 40] Rather, the MSDFT correlation functional for a given state is an implicit functional of the multistate density (eq 11), and the correlation functional developed for KS-DFT is used solely to

approximate the correlation energy of a single-determinant state (diagonal terms), an element of the Hamiltonian matrix density functional $\boldsymbol{\mathcal{H}}[\boldsymbol{D}]$. For spin-pairing interactions, the off-diagonal terms of $\boldsymbol{\mathcal{H}}[\boldsymbol{D}]$, *i.e.*, the TDF energies, are determined consistently with the all spin-up triplet state, $|1,1>$, for which, unlike the $|1,0>$ multiplet, a one determinant treatment is sufficient.[55] If one considers HKS-DFT to be an exact theory for the lowest energy state of a given spin manifold,[66] the singlet state resulting from spin coupling of two mixed-spin states is uniquely determined, consistent with the triplet-state energy, by virtue of spin-multiplet energy degeneracy, $(|1,1>) = E(|1,0>)$.[46, 56, 57] Consequently, we find that the difference in the ground-state energy between MSDFT and KS-DFT is quite small, keeping in mind that the KS-DFT state is included in the active space in NOSI calculations. The overall root-mean-square difference (RMSD) for all singlet states (except the triplet state of N_2, see below) is 0.00059 a.u. (0.017 eV). Of all structures, only formaldehyde (CH_2=O) and ammonia (NH_3) exhibit noticeable multiconfiguration contribution in the singlet states. Nevertheless, the NOSI ground states for formaldehyde and ammonia are overwhelmingly composed of the KS-configuration, respectively having 99.7% and 99.6% in configuration weight.[67] Without these two states, the RMSD is reduced to 0.00030 a.u. (0.008 eV) relative to single-determinant, KS-DFT energies. For the triplet states, the same trend is observed and only hydrogen sulfide (H_2S) shows some multiconfigurational contributions over the KS-DFT energy (Table 1). The triplet state of dinitrogen was excluded in the statistics because the lowest triplet state is the multiconfigurational $\pi \rightarrow \pi^*$ transition, in accord with the TBE from WFT,[13] but the $n \rightarrow \pi^*$ state has the lowest energy from a single-determinant optimization using KS-DFT.

The data in Table 2 show that double counting of static correlation embedded in multiconfiguration interaction in MSDFT-NOSI is minimal as tested over the molecules in the Loos2018 dataset using the M06-2X functional for the diagonal elements of the HMDF.

Furthermore, the multistate energies for both singlet and triplet states have the same RMSD of 0.016 eV from the corresponding KS-DFT results. Importantly, state interaction in MSDFT ensures that all adiabatic states are orthogonal in contrast to state-specific optimization.

Table 2. Computed total energies (a.u.) for the singlet and triplet ground states and difference from Kohn-Sham density functional theory.[a]

Molecule	S_0		T_1	
	MSDFT	ΔE_{KS}	MSDFT	ΔE_{KS}
H_2O	-76.43070	-0.00048	-76.15937	0.00000
H_2S[b]	-399.39358	-0.00019	-399.18412	-0.00239
NH_3	-56.55466	-0.00148	-56.31586	-0.00001
HCl	-460.80965	0.00000	-460.53647	0.00000
HC≡CH	-77.32602	0.00000	-77.11100	0.00000
$H_2C=CH_2$	-78.57326	0.00000	-78.40807	0.00000
Cyclopropane[b]	-116.61033	0.00000	-116.45067	0.00000
$H_2C=O$	-114.50102	-0.00169	-114.37185	0.00000
$CH_3CH=O$[c]	-153.78187	-0.00063	-153.63980	-0.00006
$CH_2=C=O$[c]	-152.56190	0.00000	-152.42677	0.00000
$HCONH_2$[c]	-169.85401	-0.00052	-169.65987	-0.00003
$H_2C=S$	-437.45851	0.00000	-437.39160	0.00000
$CH_2=NH$	-94.62199	-0.00012	-94.45830	-0.00001
CH_3-N=O	-169.79038	-0.00054	-169.75579	-0.00009
$H_2C=N_2$	-148.73554	-0.00044	-148.63877	0.00020
streptocyanine	-150.37478	0.00000	-150.17170	0.00000
CO	-113. 32105	-0. 00000	-113.09571	0.00000
N_2	-109.53515	-0.00002	-109.25536	-.015026

a. The Minnesota M06-2X density functional is used in MSDFT-NOSI and Kohn-Sham DFT calculations. Energy differences between MSDFT and KS-DFT are given as $\Delta E_{KS} = E_{MSDFT} - E_{KSDFT}$. The aug-cc-pVTZ basis function is used. b. The cc-pVQZ basis set is used. c. The aug-cc-pVDZ basis set is used.

B. Performance of NOSI with the M06-2X Functional. We next examine the performance of MSDFT using nonorthogonal state interaction with a standard meta-GGA density functional approximation developed for the ground state KS-DFT, in particular, the Minnesota M06-2X functional.[41] The excitation energies from MSDFT-NOSI calculations are compared against the Loos2018 dataset in Figure 1, in which three computational procedures are examined, differing in state optimization and TDF approximation. We first optimize the determinant configurations in the MAS for each molecule using either the BLE[52] or the TSO method.[53, 54] Then, we enforce the spin multiplet-energy degeneracy of the triplet state $|1,1>$ (identically $|1,-1>$) with that of the multiconfigurational $|1,0>$ state resulting from spin-coupling interaction.[46, 56] This constraint uniquely determines the TDF value (eq 13), even in the absence of an explicit functional expression for TDF between spin-pairing interactions, and it is denoted as spin-multiplet degeneracy (SMD). Along with the two optimization methods, we have the MSD-BLE and MSD-TSO computational models.

Alternatively, we also examine the performance of MSDFT-NOSI in which the SMD condition is not enforced. Thus, we employ the expression in eq 14, featuring an overlap-scaled average (OSA) correlation-energy of two interacting states, to approximate the TDF for all off-diagonal terms of $\boldsymbol{\mathcal{H}}[\boldsymbol{D}]$. Equation 14 was initially proposed as an ad-hoc approximation without rigorous justification,[33] but we now know that it is the leading term of an expression for the TDF in order to satisfy the matrix functional transformation property of the HMDF[28, 29] when the KS-DFT correlation energy for each configuration is used in the diagonal term.[40] In this work, OSA is evaluated on the states optimized using the BLE method, and this procedure is termed as OSA-BLE.

Comparison between results obtained using the SMD-BLE and SMD-TSO approaches gives an indication of the effect of orbital-occupation constraint in the TSO method on the overall adiabatic excitation energy. On the other hand, comparison between results from the SMD-BLE and OSA-BLE highlights the significance of meeting certain physical conditions in constructing explicit transition density functionals in the future.

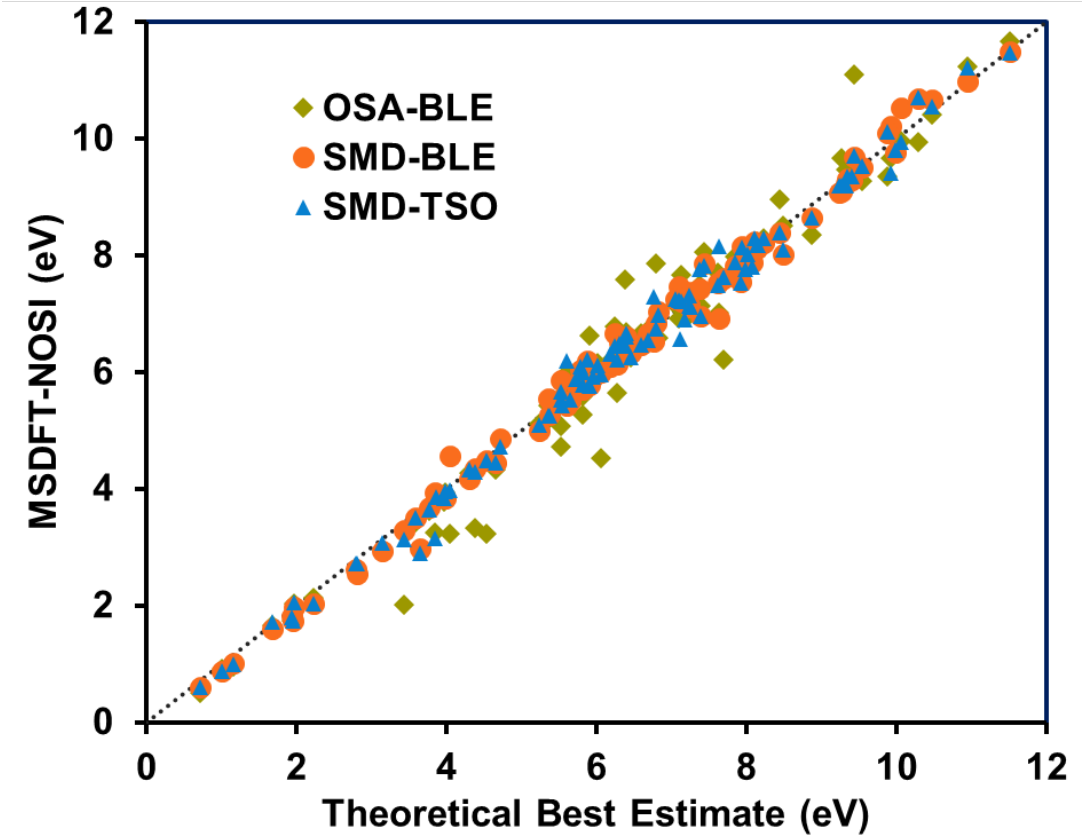

Figure 1. Excitation energies of both singlet and triplet states from multistate density functional theory (MSDFT) with nonorthogonal state interaction (NOSI) against the theoretical best estimates of the Loos2018 dataset. The block-localized excitation (BLE) and target state optimization (TSO) methods are used to determine the basis-state configurations along with the spin multiplet-energy degeneracy (SMD) and the overlap-scaled average (OSA) correlation approximation for constructing the Hamiltonian matrix density functional.

Depicted in Figure 1 are 100 excitation energies for the eighteen compounds from the Loos2018 dataset[13] against values computed using MSDFT-NOSI with the M06-2X density functional, excluding a few high-energy states that are not sufficiently represented by the present MAS (Table 1). The overall agreement between MSDFT results and the Loose2018 benchmark is good for the SMD method either with the BLE or with the TSO optimization techniques. The root-mean-square errors (RMSE) are 0.22 and 0.24 eV, respectively, for the SMD-BLE and SMD-TSO model. The corresponding mean signed errors (MSE) and mean absolute errors (MAE) are -0.02 and -0.01 eV, and 0.17 and 0.18 eV for the two methods. Consequently, one finds that there is little systematic error in both models. On the other hand, the computed excitation energies using the OSA-BLE approach show somewhat greater fluctuations; RMSE, MSE and MAE are, respectively, 0.48, -0.07 and 0.31 eV. Therefore, there is a clear advantage to restricting the TDF correlation energy between two spin-pair configurations to match the energy of the multiconfigurational $|1,0>$ state to the corresponding $|1,1>$ triplet state. It may be argued that an additional KS-DFT calculation is needed for the all spin-up triplet state in the SMD model, but the extra cost is practically negligible.

Loos et al. evaluated a list of 12 popular computational methods.[13] Couple-cluster with triple excitations including CCSDT, CCSDTQ and CC3 have the best performance with an RMSE of 0.04 eV or less, whereas the popular ADC(2) and ADC(3) as well as CC2 exhibit larger deviations at about 0.28 eV. However, several cases including doubly excited state and states involving strong state mixing were excluded in the statistics in that analysis.[13] MSDFT-NOSI, coupled with a popular density functional approximation (M06-2X) developed for KS-DFT, can yield results lying between the most accurate CC series that include triples and those cost-efficient, second-order wave function theories. Similar to the findings in the 2018 investigation of wave

function methods,[13] we also found no notable difference in accuracy for MSDFT-NOSI between singlet and triplet excitations. For WFT, the low-cost models, CIS(D), CIS(D_∞), ADC(2) and CC2, have greater average errors (MAE) in Rydberg states by as much as 0.15 eV than valence excited states. In the present analysis, a total of 57 valence excited states and 43 Rydberg states are included. It turns out that NOSI(SMD) performs slightly better for the Rydberg states (MAE: 0.15 eV; RMSE: 0.19 eV) than valence excitations (MAE: 0.18 eV; RMSE: 0.24 eV). This trend mirrors that of the ADC(3) method (MAE of 0.17 eV and 0.28 eV, respectively) found in the Loos2018 study.[13] The main source of errors in valence excitation in the present NOSI method comes from $\pi \rightarrow \pi^*$ transitions. We noticed previously that the errors in the two simplest unsaturated hydrocarbons can be significantly reduced if an alkyl substitution is added; a detailed investigation is beyond the scope of this work. Thus, in practice, the errors on low-energy valence excitations can be significantly smaller than the benchmark comparison.

In Table 3, we list the computed excitation energies using MSDFT-NOSI along with those from the reference TBE and the CC3 method in the Loos2018 dataset[13] and TDDFT values with the M06-2X functional. The computed oscillator strengths along with those from the Loos benchmark are also listed, but no further comments will be made. Below, we briefly examine the performance of NOSI on different classes of molecules. Here, we focus on results obtained using the M06-2X functional and the SMD approach for estimating TDF contributions.

Table 3: Computed Excitation Energies (eV) and Oscillator Strengths using Multistate Density Functional Theory Along With the Theoretical Best Estimates (TBE) and CC3 from the Loos2018 Database, and TDDFT Values.[a]

Molecule	State	Loos2018		M06-2X			PBE0		Oscillator Strength	
		TBE	CC3	SMD-BLE	SMD-TSO	OSA-BLE	TDDFT	SMD-BLE	SMD-TSO	Loos2018
H_2O	$^1B_1$ ($n \rightarrow 3s$)	7.62	7.60	7.53	7.49	7.70	7.46	7.38	0.033	0.054
	$^1A_2$ ($n \rightarrow 3p$)	9.41	9.38	9.30	9.36	9.33	8.93	8.82	0.000	
	$^1A_1$ ($n \rightarrow 3s$)	9.99	9.97	9.76	9.80	10.00	9.64	9.78	0.148	0.100
	$^3B_1$ ($n \rightarrow 3s$)	7.25	7.23	7.38	7.11	7.22	7.37	7.02	0.033	
	$^3A_2$ ($n \rightarrow 3p$)	9.24	9.22	9.08	9.20	9.06	9.14	8.45		
	$^3A_1$ ($n \rightarrow 3s$)	9.54	9.52	9.51	9.52	9.27	9.38	9.26		
NH_3	$^1A_2$ ($n \rightarrow 3s$)	6.59	6.57	6.47	6.47	6.67	6.41	6.43	0.095	0.086
	^1E ($n \rightarrow 3p$)	8.16	8.15	8.16	8.18	8.17	7.68	7.81	0.006	0.006
	$^1A_1$ ($n \rightarrow 3p$)	9.33	9.32	9.24	9.20	9.48	9.04	8.93	0.006	0.003
	$^3A_2$ ($n \rightarrow 3s$)	6.31	6.29	6.50	6.50	6.30	6.46	6.16		
H_2S[b]	$^1A_2$ ($n \rightarrow 4p$)	6.18	6.19	6.09	6.31	6.19	5.88	5.68	0.000	
	$^1B_1$ ($n \rightarrow 4s$)	6.24	6.24	6.66	6.44	6.79	5.99	6.13	0.060	0.063
	$^3A_2$ ($n \rightarrow 4p$)	5.81	5.82	5.70	6.00	5.59	5.84	5.43		
	$^3B_1$ ($n \rightarrow 4s$)	5.88	5.88	6.20	6.20	6.16	6.04	5.68		
HCl	$^1\Pi$ (CT)	7.84	7.84	7.83	7.87	7.97	7.56	7.51	0.006	0.056
HC≡CH	$^1\Sigma^-_u$ ($\pi \rightarrow \pi^*$)	7.10	7.09	7.46	7.24	6.92	6.00	7.32	0.596	
	$^1\Delta_u$ ($\pi \rightarrow \pi^*$)	7.44	7.42	7.87	7.82	8.05	7.07	7.72	0.632	
	$^3\Sigma^+_u$ ($\pi \rightarrow \pi^*$)	5.53	5.50	5.85	5.66	4.73	5.34	5.48		
	$^3\Delta_u$ ($\pi \rightarrow \pi^*$)	6.40	6.40	6.37	6.66	6.39	6.37	6.21		
	^1A_u (F; $\pi \rightarrow \pi^*$)	3.64	3.64	2.98	2.90	2.97	2.29	2.77	0.017	
	$^1A_2$ (F; $\pi \rightarrow \pi^*$)	3.85	3.84	3.94	3.15	3.25	4.11	3.83	0.000	
CH_2=CH_2	$^1B_{3u}$ ($\pi \rightarrow 3s$)	7.39	7.35	6.96	6.96	7.14	6.94	7.07	0.110	0.078
	$^1B_{1u}$ ($\pi \rightarrow \pi^*$)	7.93	7.91	7.54	7.53	7.80	7.47	7.42	0.720	0.346
	$^1B_{1g}$ ($\pi \rightarrow 3p$)	8.08	8.03	7.88	7.81	7.91	8.00	7.70	0.000	
	$^3B_{1u}$ ($\pi \rightarrow \pi^*$)	4.54	4.53	4.49	4.48	3.22	4.50	4.25		
	$^3B_{3u}$ ($\pi \rightarrow 3s$)	7.23	7.24	7.15	7.14	6.97	6.76	6.87		
	$^3B_{1g}$ ($\pi \rightarrow 3p$)	7.98	7.98	7.84	7.76	7.81	7.25	7.59		

Cyclopropene[b]	$^1B_1$ ($\sigma \rightarrow \pi^*$)	6.68	6.68	6.66	6.56	6.73	6.37	6.25	0.009	0.001
	$^1B_2$ ($\pi \rightarrow \pi^*$)	6.79	6.73	6.85	6.74	7.87	6.55	6.51	0.367	0.071
	$^3B_2$ ($\pi \rightarrow \pi^*$)	4.38	4.34	4.34	4.30	3.32	4.34	3.97		
	$^3B_1$ ($\sigma \rightarrow \pi^*$)	6.45	6.43	6.33	6.24	6.26	6.27	6.03		
CH_2=O	$^1A_2$ ($n \rightarrow \pi^*$)	3.98	3.97	3.84	3.95	3.94	3.68	3.82	0.000	
	$^1B_2$ ($n \rightarrow 3s$)	7.23	7.18	7.11	7.31	7.20	7.17	7.01	0.036	0.021
	$^1A_1$ ($\pi \rightarrow \pi^*$)	9.43	9.48	9.68	9.71	11.10	9.39	9.68	0.637	0.135
	$^1B_2$ ($n \rightarrow 3p$)	8.13	8.07	8.12	8.18	8.24	7.97	8.17	0.030	0.037
	$^1A_1$ (n $\rightarrow$ 3 p)	8.23	8.18	8.21	8.30	8.30	8.05	8.17	0.068	0.052
	$^3A_2$ ($n \rightarrow \pi^*$)	3.58	3.57	3.51	3.49	3.42	3.47	3.52		
	$^3A_1$ ($\pi \rightarrow \pi^*$)	6.06	6.05	6.00	5.96	4.52	5.50	6.09		
	$^3B_2$ ($n \rightarrow 3s$)	7.06	7.03	7.26	7.24	7.16	6.82	6.85		
	$^3B_2$ ($n \rightarrow 3p$)	7.94	7.92	8.16	8.14	8.04	7.55	8.02		
	$^3A_1$ ($n \rightarrow 3p$)	8.10	8.08	8.24	8.30	8.14	7.64	8.07		
	$^1A''$ (F; $n \rightarrow \pi^*$)	2.80	2.84	2.55	2.73	2.61	2.64	2.29	0.001	
CH_3CH=O[c]	$^1A"$ ($n \rightarrow \pi^*$)	4.31	4.31	4.18	4.33	4.27	3.97	3.85	0.000	0.000
	$^3A"$ ($n \rightarrow \pi^*$)	3.97	3.95	3.87	3.84	3.77	3.85	3.59	0.000	
CH_2=C=O[c]	$^1A_2$ ($\pi \rightarrow \pi^*$)	3.86	3.88	3.85	3.85	3.90	3.69	3.52	0.000	
	$^1B_1$ ($\pi \rightarrow 3s$)	6.01	5.96	6.00	6.11	6.15	5.87	5.96	0.061	0.035
	$^1A_2$ ($\pi \rightarrow 3p$)	7.18	7.16	7.27	6.90	7.29	6.85	6.96	0.711	
	$^3A_2$ ($\pi \rightarrow \pi^*$)	3.77	3.78	3.68	3.65	3.62	3.65	3.46		
	$^3B_1$ ($\pi \rightarrow 3s$)	5.79	5.76	6.03	6.10	5.87	5.73	5.75		
	$^3A_2$ ($\pi \rightarrow 3p$)	7.12	7.12	7.25	6.56	7.24	6.74	6.92		
	$^1A''$ (F; $\pi \rightarrow \pi^*$)	1.00	1.00	0.87	0.88	0.91	0.79	0.64	0.001	
$HCONH_2$[c]	$^1A"$ ($n \rightarrow \pi^*$)	5.65	5.66	5.51	5.53	5.59	5.43	5.22	0.002	0.000
	$^1A'$ ($n \rightarrow 3s$)	6.77	6.74	6.52	7.30	6.72	6.77	6.12	0.093	0.001
	$^1A'$ ($\pi \rightarrow \pi^*$)	7.63	7.62	6.92	8.16	7.01	7.01	6.73	0.023	0.251
	$^1A'$ ($n/\pi \rightarrow 3p$)	7.38	7.40	7.42	7.77	7.49	7.52	7.47	0.131	0.111
	$^3A"$ ($n \rightarrow \pi^*$)	5.38	5.38	5.28	5.25	5.21	4.94	5.02		
	$^3A'$ ($\pi \rightarrow \pi^*$)	5.81	5.82	5.80	5.79	5.27	5.80	5.43		
CH_2=S	$^1A_2$ ($n \rightarrow \pi^*$)	2.22	2.23	2.04	2.03	2.13	2.01	1.77	0.000	
	$^1B_2$ ($n \rightarrow 4s$)	5.96	5.91	5.91	5.91	6.00	5.75	5.78	0.026	
	$^1A_1$ ($\pi \rightarrow \pi^*$)	6.38	6.48	6.31	6.45	7.58	6.20	6.06	0.751	0.178

	$^3A_2$ ($n \rightarrow \pi^*$)	1.94	1.94	1.82	1.79	1.74	1.83	1.60		
	$^3A_1$ ($\pi \rightarrow \pi^*$)	3.43	3.38	3.28	3.13	2.00	3.17	3.09		
	$^3B_2$ ($n \rightarrow 4s$)	5.72	5.72	5.81	5.88	5.72	5.56	5.48		
	^{1}A$_2$ (F; $n \rightarrow \pi^*$)	1.95	1.97	1.74	1.74	1.81	1.81	1.51	0.000	
CH_2=NH	$^1A''$ ($n \rightarrow \pi^*$)	5.23	5.20	4.99	5.09	5.11	4.89	4.69	0.008	0.003
	$^3A''$ ($n \rightarrow \pi^*$)	4.65	4.61	4.45	4.45	4.33	4.46	4.19		
CH_3-N=O	$^1A''$ ($n \rightarrow \pi^*$)	1.96	1.96	1.98	2.06	2.03	1.31	1.56	0.001	0.000
	$^1A'$ (n, $n \rightarrow \pi^*$,π^*)	4.72	5.76	4.85	4.72	4.85	6.42	4.86	0.000	0.000
	$^1A'$ ($n \rightarrow 3s/3p$)	6.40	6.31	6.61	6.61	6.69	6.32	6.26	0.005	0.006
	$^3A''$ ($n \rightarrow \pi^*$)	1.16	1.14	1.01	1.00	0.95	0.93	0.85		
	$^3A'$ ($\pi \rightarrow \pi^*$)	5.60	5.51	5.42	6.19	5.98	4.79	5.15		
	$^1A''$ (F; $n \rightarrow \pi^*$)	1.67	1.69	1.60	1.71	1.66	0.92	1.18	0.001	
CH_2-N_2	$^1A_2$ ($\pi \rightarrow \pi^*$)	3.14	3.07	2.93	3.07	2.93	2.73	2.67	0.000	
	$^1B_1$ ($\pi \rightarrow 3s$)	5.54	5.45	5.48	5.42	5.60	5.25	5.46	0.263	0.002
	$^1A_1$ ($\pi \rightarrow \pi^*$)	5.9	5.84	5.79	5.77	6.63	5.79	5.91	0.086	0.210
	$^3A_2$ ($\pi \rightarrow \pi^*$)	2.79	2.83	2.63	2.72	2.63	2.62	2.49		
	$^3A_1$ ($\pi \rightarrow \pi^*$)	4.05	4.03	4.57	3.97	3.23	3.58	3.73		
	$^3B_1$ ($\pi \rightarrow 3s$)	5.35	5.31	5.55	5.25	5.42	5.28	5.29		
	$^3A_1$ ($\pi \rightarrow \pi^*/3p$)	6.82	6.80	7.04	6.97	6.59	6.18	6.30		
	$^3A''$ (F; $\pi \rightarrow \pi^*$)	0.71	0.68	0.60	0.60	0.50	0.44	0.71	0.000	
Streptocyanine	$^1B_2$ ($\pi \rightarrow \pi^*$)	7.13	7.13	7.21	7.21	7.67	7.49	6.68	0.620	0.347
	$^3B_2$ ($\pi \rightarrow \pi^*$)	5.52	5.48	5.53	5.53	5.07	5.53	5.13	0.000	
CO	$^1\Pi$ (V; $n \rightarrow \pi^*$)	8.49	8.49	8.01	8.10	8.50	8.14	7.84	0.170	0.084
	$^1\Sigma^-$ (V; $\pi \rightarrow \pi^*$)	9.92	9.99	10.31	9.42	9.66	9.03	10.11	0.000	
	$^1\Delta$ (V; $\pi \rightarrow \pi^*$)	10.06	10.12	10.65	9.93	9.97	10.09	10.42	0.000	
	$^1\Sigma^+$ (R)	10.95	10.94	10.90	11.22	11.05	10.78	10.89	0.000	0.003
	$^1\Sigma^+$ (R)	11.52	11.49	11.51	11.48	11.65	11.16	11.30	0.000	0.200
	$^1\Pi$ (R)	11.72	11.69	11.76	11.74	11.74	11.25	11.40	0.161	0.053
	$^3\Pi$ (V; $n \rightarrow \pi^*$)	6.28	6.30	6.15	6.20	5.64	6.13	5.89		
	$^3\Sigma^+$ (V; $\pi \rightarrow \pi^*$)	8.45	8.45	8.85	8.38	8.96	7.94	8.07		
	$^3\Delta$ (V; $\pi \rightarrow \pi^*$)	9.27	9.30	9.01	9.21	9.66	8.64	8.77		
	$^3\Sigma^-$ (V; $\pi \rightarrow \pi^*$)	9.80	9.82	9.37	9.81	7.40	10.06	9.17	0.000	
	$^3\Sigma^-$ (R)	10.47	10.45	10.66	10.54	10.41	10.73	10.37		

N_2	$^1\Pi g$ (V; $n \rightarrow \pi^*$)	9.34	9.34	9.32	9.35	9.58	9.00	8.76	0.000	
	$^1\Sigma^-$ (V; $\pi \rightarrow \pi^*$)	9.88	9.88	10.09	10.11	9.35	8.38	10.07	0.000	
	$^1\Delta$ (V; $\pi \rightarrow \pi^*$)	10.29	10.29	10.69	10.71	9.95	9.93	10.68	0.000	0.000
	$^1\Sigma g^+$ (R)	12.98	13.01	12.95	12.92	13.19	12.84	12.7	0.000	
	1Πu (R)	13.03	13.22	13.43	13.72	13.6	12.96	13.09	0.096	0.229
	1Σu+ (R)	13.09	13.12	13.54	13.55	13.66	13.07	13.51	0.144	0.296
	1Πu (R;)	13.46	13.49	14.6	13.79	14.63	13.25	14.3	0.097	0.000
	3Σu+ (V; $\pi \rightarrow \pi^*$)	7.70	7.68	7.61	7.62	6.22	8.05	7.24		
	3Πg (V; n $\rightarrow \pi^*$)	8.01	8.04	8.02	8.01	7.77	8.03	7.64		
	$^3\Delta$u (V; $\pi \rightarrow \pi^*$)	8.87	8.87	8.64	8.64	8.35	8.51	8.25		
	$^3\Sigma u^-$ (V; $\pi \rightarrow \pi^*$)	9.66	9.68	8.90	8.90	9.38	8.55	8.80		

a. aug-cc-pVTZ basis set used in all calculations, except noted. Loos2018: Loos, P. F., et al. 2018, reference 13. CC3: third-order response coupled cluster. TDDFT: time-dependent density functional theory. SMD: spin-multiplet degeneracy. OSA: overlap-scaled average. BLE: block-localized excitation. TSO: target state optimization. b. cc-pVQZ basis set. c. aug-cc-pVDZ basis set.

Four small hydrogenic compounds (H_2O, H_3N, H_2S and HCl) comprising 15 excited states are included in the benchmark set. The agreement between NOSI results and the TBE values is excellent, with the largest errors for the n→4s singlet (0.42 eV) and triplet (0.32 eV) states of H_2S, without which the MAE is 0.10 eV for the hydrogenic molecules using either BLE and TSO optimizations. Undoubtedly, larger basis sets are needed to better describe higher-energy Rydberg states.

There are three unsaturated hydrocarbon compounds in the Loos2018 dataset, including acetylene, ethylene and cyclopropene. The overall MAEs are 0.21 and 0.27 eV for the SMD-BLE and SMD-TSO model, respectively, including 16 excited states and two transition energies at the excited state geometry. The two smallest alkyne and alkene compounds turn out to be most difficult for NOSI with relatively large errors in valence excitations greater than the average performance for the entire dataset. This is unfortunate in benchmark studies since the performance of NOSI on substitute alkenes and alkynes can be better.

Four carbonyl compounds with 26 excited states are included in the test set (formaldehyde, acetaldehyde, ketene, and formamide). Of these compounds, greater errors are found in formamide, especially on the high-lying $\pi \rightarrow \pi^*$ transition with an error as large as -0.71 eV in SMD-BLE and +0.53 eV in SMD-TSO. Nevertheless, the overall performance of NOSI/SMD-BLE is generally reasonable with an MAE of 0.12 eV on the SMD-BLE energies and 0.17 eV on SMD-TSO results, excluding the $\pi \rightarrow \pi^*$ state of formamide. The characteristic $n \rightarrow \pi^*$ transitions of formaldehyde, acetaldehyde and formamide are underestimated by 0.13 eV relative to the corresponding TBE, but the result for ketene is within 0.01 eV.

The excitation energies determined for the isoelectronic diatomic molecules CO and N_2 feature a variety of transitions, including $n \rightarrow \pi^*$, $\pi \rightarrow \pi^*$ and Rydberg states, of which several

states involve state interactions. The average error for the 18 transition energies shown in Table 3 is 0.21 eV for both SMD-BLE and SMD-TSO methods, greater than the overall statistical average of all compounds. Here, a number of Rydberg states and $\pi \rightarrow \pi^*$ transitions have similar energies which become sensitive to the range of configurations in the active space (Table 1). The difficulty also highlights the limitations of the present nonorthogonal state interaction method, which is effective for systems with a limited number of low-lying states. As the energy difference between different excited states gets smaller, it becomes difficult to optimize individual configurational states with a given non-aufbau occupation. Therefore, an alternative approach such as the multiconfiguration self-consist-field with singles and doubles (SDSCF) method described previously may be desired for high-energy excitations where state separation becomes small.[39]

The remaining compounds in the benchmark set are five species containing somewhat exotic functional groups; they are CH_2=NH, CH_2=N_2, CH_3-NO, CH_2=S, and H_2N-CH=NH_2^+ (streptocyanine). Several excited states of diazomethane have errors above average with the largest (0.52 eV) for the $^3A_1$ $\pi \rightarrow \pi^*$ transition. Three other states having errors greater than 0.2 eV are the $n \rightarrow \pi^*$ transition of CH_2=NH, the $n \rightarrow 3s/3p$ Rydberg state of CH_3-NO, and the fluorescent transition of CH_2=S. The mean-absolute error in the 25 excitation energies of the five compounds is 0.15 eV employing the SMD-BLE method. The same performance is found in the SMD-TSO approach.

C. Comparison with TDDFT and PBE0 Functional. To shed light on the performance of MSDFT, we also include the results of NOSI using the hybrid PBE0 density functional approximation and data from linear-response time-dependent density functional theory. The SMD-BLE model is used in NOSI/PBE0 calculations. Except for cases involving double excitation, strong state mixing and significant charge-transfer contribution, the results from TDDFT should

be quite good for the small organic molecules in the Loos2018 dataset. Comparison of MSDFT and TDDFT against a common set of best theoretical estimates on excitation energies (Figure 3) can provide a direct assessment of the scope and accuracy of MSDFT relative to a well-established and widely used method,[25] whereas the comparison between MSDFT results obtained by using different density functional approximations (Figure 3) reminds us of the importance to develop novel density functional approximations suitable for both the ground state and excited states.

Table 4. Mean Signed Errors (MSE), Mean Absolute Errors (MAE), Root-Mean-Square Errors (RMSE), and Maximum Deviations of Computed Excitation Energies (in eV) Obtained by Using the MSDFT-NOSI and TDDFT Methods Against Theoretical Best Estimates of the Loos2018 Benchmark.[a]

Method	No. of states	MSE	MAE	RMSE	Max(+)	Max(-)
ADC(3)	106	-0.15	0.23	0.28	-0.79	0.39
CC2	106	0.03	0.22	0.28	-0.71	0.63
CC3	106	-0.01	0.03	0.04	-0.09	0.19
CCSD	106	0.05	0.08	0.11	-0.17	0.40
CCSDT	104	-0.01	0.03	0.03	-0.10	0.11
SMD-BLE	100	-0.02	0.17	0.22	-0.71	0.59
SMD-TSO	100	-0.01	0.18	0.24	-0.74	0.69
OSA-BLE	100	-0.07	0.31	0.48	-1.54	1.61
SMD/PBE0	100	-0.26	0.31	0.36	-0.91	0.42
TDDFT	100	-0.24	0.31	0.42	-1.50	1.70

a. Data on wave function theories (ADC, CC2, CC3, CCSD and CCSDT) taken from ref. [13].

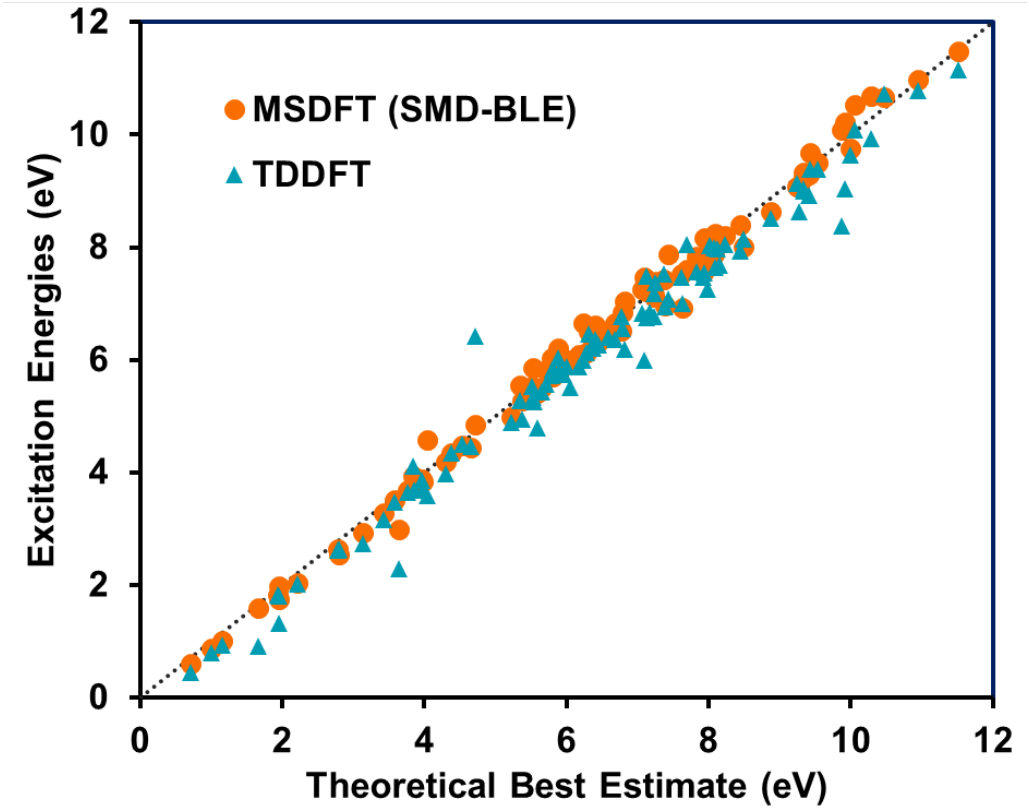

Figure 2. Comparison of excitation energies (eV) determined using multistate multistate density functional theory (MSDFT) with nonorthogonal state interaction (NOSI) and time-dependent density functional theory (TDDFT) against a set of best theoretical estimates of the Loos2018 dataset. The M06-2X functional is used both in MSDFT and in TDDFT calculations.

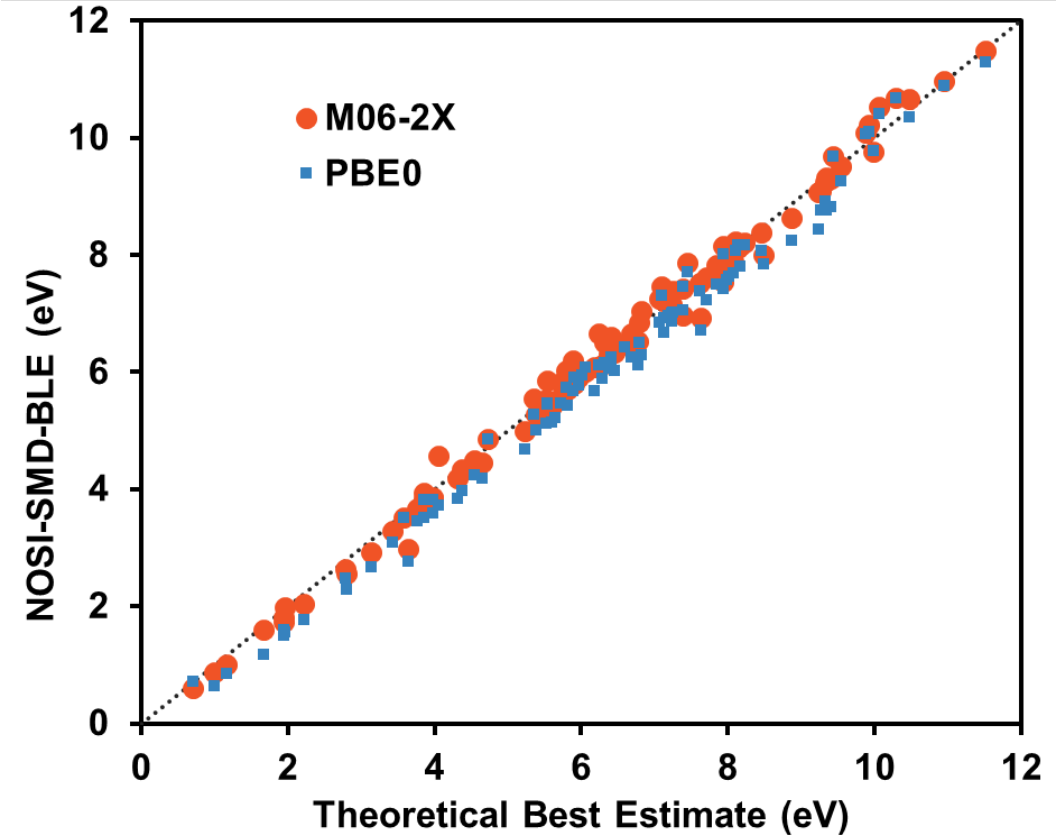

Figure 3. Comparison of excitation energies (eV) determined using multistate multistate density functional theory (MSDFT) with nonorthogonal state interaction (NOSI). The M06-2X and PBE0 density functionals are used.

By inspection of Figures 2 and 3, one immediately notices that both TDDFT/M06-2X and NOSI/PBE0 systematically underestimate the excitation energies against the TBE data. Indeed, the MSE is -0.24 eV for TDDFT/M06-2X and -0.26 eV on the NOSI/PBE0 results. This is markedly different from a MSE of -0.02 eV in the NOSI/M06-2X results. The systematic trends are also revealed in the MAE and RMSE for the two sets of data, which are, respectively, 0.31 eV and 0.42 eV for TDDFT, and 0.31 eV and 0.36 eV for NOSI/PBE0. One special outlier in TDDFT results is the $(n, n \rightarrow \pi^*, \pi^*)$ double-excitation state of nitrosomethane (Figure 2), which has a a value of 6.42 eV from TDDFT/M06-2X, but the theoretical best estimate is 4.72 eV. The similarity in magnitude between MSE and MAE for both TDDFT/M06-2x and NOSI/PBE0 methods further

confirms the visual depiction in Figures 2 and 3. Overall, we can draw two conclusions: (a) NOSI with SMD-BLE (and SMD-TSO) outperforms TDDFT substantially using the same density functional approximation (M06-2X) on the Loos2018 dataset, and (b) the accuracy of NOSI calculations is dependent on the particular density functional approximation used. In the latter case, the use of PBE0 functional for the diagonal terms of $\boldsymbol{\mathcal{H}}[\boldsymbol{D}]$ leads to a greater average error (0.31 eV) than that by using M06-2X (0.17 eV).

5. Conclusions

In this work, we examine the performance of multistate density functional theory with nonorthogonal state interaction (MSDFT-NOSI) for excitation energy calculations beyond the traditional TDDFT and HKS-DFT for the ground state. MSDFT-NOSI is based on the theorems of Lu and Gao,[28] who established the existence of a Hamiltonian matrix density functional of state and transition densities. Importantly, the matrix density for the lowest N states of a molecular system can be represented by no more than N^2 Slater determinants, defining an upper bound in the number of configuration states and the possibility of constructing a minimal active space (MAS) for a given number of adiabatic states of interest. Two optimization methods are used to determine the basis configuration states, namely the block-localized excitation (BLE) and the target state optimization (TSO) techniques. Furthermore, we employ two ways of approximating the transition density functional (TDF) for the correlation energy of the off-diagonal terms of the HMDF. MSDFT-NOSI is assessed for 100 excitation energies in the 2018 dataset by Loos et al. (Loos2018) taken from a series of high-quality theoretical best estimates on a wide range of compounds.[13-17]

We made the following main findings.

1. MSDFT-NOSI is generally more accurate than TDDFT using the Minnesota M06-2X functional on the Loos2018 dataset. Both the BLE and TSO optimization techniques yield similar results with RMSE of 0.22 eV and 0.24 eV, respectively, compared to an RMSE of 0.43 eV for TDDFT.
2. In comparison of the total energies for the ground state from the multistate MSDFT-NOSI and the single-determinant KS-DFT calculations, we found that there is little double counting of correlation in the multistate approach. The mean signed difference (MSD) and root-mean-square difference (RMSD) between the multistate and non-interacting reference approaches are -0.00025 and 0.00059 a.u. (less than 0.016 eV), respectively. Thus, it is encouraging to make use of the vast toolset developed for KS-DFT, and to develop novel matrix density functionals to study the ground state and excited states.
3. There are no systematic errors in the computed excitation energies using MSDFT-NOSI with M06-2X functional. The mean signed errors (MSE) are -0.02 eV and -0.01 eV using the BLE and TSO optimization method.
4. The performance of MSDFT-NOSI on excited-state calculations depends on the specific functional used as that of TDDFT. Of the two functionals examined, PBE0 shows a greater average error with an RMSE of 0.36 eV compared to that of 0.22 eV for M06-2X. However, the error is systematic with a linear regression slope of 0.994 and an intercept of 0.28 on an $R^2 = 0.998$.
5. Of the Loos2018 excited-state database, MSDFT-NOSI/M06-2X has an RMSE of 0.22 eV, which is better than ADC(3) and CC2 (both 0.28 eV), but greater than CCSD (0.11 eV) and CC3 (0.04 eV). It also performs better than the best functionals in TDDFT/TDA benchmarks by Head-Gordon and coworkers (RMSEs of 0.25-0.3 eV) on a different, larger set of targets.

6. All things considered; we recommend MSDFT-NOSI/M06-2X for excited state calculations with the SMD estimates for TDF between spin coupled configurations.

Hohenberg-Kohn-Sham density functional theory for the ground state has revolutionized modern model chemistry, balancing accuracy and efficiency, whereas TDDFT offers excellent excitation energies for many systems. However, the latter also suffers from numerous well-known shortcomings, including the double-excitation state of nitrosomethane in the Loos2018 dataset. MSDFT is a rigorous density functional theory for all states. We found that the density functional approximations developed for HKS-DFT can be adopted to MSDFT-NOSI calculations of excited states, exhibiting a performance better than that of TDDFT using the same functional approximation on a carefully constructed high-quality database. The present benchmark study further sheds light on the possibility to develop explicit and accurate matrix density functionals both for the ground state and for excited states without relying on time-dependent approaches.

Acknowledgments: This work has been partially supported by the Shenzhen Municipal Science and Technology Innovation Commission (KQTD2017-0330155106581) and the Key-area Research and Development Program of Guangdong Province (2020B0101350001). Computations performed at Minnesota was supported by the National Institutes of Health (GM046716).

AUTHOR INFORMATION

Corresponding Authors

Meiyi Liu – Institute of Systems and Physical Biology, Shenzhen Bay Laboratory, Shenzhen 518055, China; Email: liumy@szbl.ac.cn;

Jun Zhang – Institute of Systems and Physical Biology, Shenzhen Bay Laboratory, Shenzhen 518055, China; Email: zhangjun@szbl.ac.cn;

Jiali Gao − Institute of Systems and Physical Biology, Shenzhen Bay Laboratory, Shenzhen 518055, China; School of Chemical Biology & Biotechnology, Peking University Shenzhen Graduate School, Shenzhen, Guangdong 518055, China; Department of Chemistry and Supercomputing Institute, University of Minnesota, Minneapolis, Minnesota 55455, United States; orcid.org/0000-0003-0106-7154; Email: gao@ jialigao.org;

Authors

Hong Zhu – School of Chemical Biology & Biotechnology, Peking University Shenzhen Graduate School, Shenzhen, Guangdong 518055, China; Institute of Systems and Physical Biology, Shenzhen Bay Laboratory, Shenzhen, Guangdong Province 518055, China;

Ruoqi Zhao – Institute of Systems and Physical Biology, Shenzhen Bay Laboratory, Shenzhen, Guangdong Province 518055, China;

Notes

The authors declare no competing financial interests.

References:

(1) Pople, J. A.; Head-Gordon, M.; Fox, D. J.; Raghavachari, K.; Curtiss, L. A. Gaussian-1 Theory - a General Procedure for Prediction of Molecular-Energies. *J. Chem. Phys.* **1989**, *90*, 5622-5629.

(2) Curtiss, L. A.; Raghavachari, K.; Trucks, G. W.; Pople, J. A. Gaussian-2 Theory for Molecular-Energies of 1st-Row and 2nd-Row Compounds. *J. Chem. Phys.* **1991**, *94*, 7221-7230.

(3) Curtiss, L. A.; Raghavachari, K.; Redfern, P. C.; Rassolov, V.; Pople, J. A. Gaussian-3 (G3) theory for molecules containing first and second-row atoms. *J. Chem. Phys.* **1998**, *109*, 7764-7776.

(4) Curtiss, L. A.; Redfern, P. C.; Raghavachari, K. Gaussian-4 theory. *J. Chem. Phys.* **2007**, *126*, 084108.

(5) Schreiber, M.; Silva-Junior, M. R.; Sauer, S. P. A.; Thiel, W. Benchmarks for electronically excited states: CASPT2, CC2, CCSD, and CC3. *J. Chem. Phys.* **2008**, *128*, 134110/134111-134110/134125.

(6) Silva, M. R.; Schreiber, M.; Sauer, S. P. A.; Thiel, W. Benchmarks of electronically excited states: Basis set effects on CASPT2 results. *J. Chem. Phys.* **2010**, *133*, 174318.

(7) Silva-Junior, M. R.; Sauer, S. P. A.; Schreiber, M.; Thiel, W. Basis set effects on coupled cluster benchmarks of electronically excited states: CC3, CCSDR(3) and CC2. *Mol. Phys.* **2010**, *108*, 453-465.

(8) Schapiro, I.; Sivalingam, K.; Neese, F. Assessment of n-Electron Valence State Perturbation Theory for Vertical Excitation Energies. *J. Chem. Theory Comput.* **2013**, *9*, 3567-3580.

(9) Piecuch, P.; Hansen, J. A.; Ajala, A. O. Benchmarking the completely renormalised equation-of-motion coupled-cluster approaches for vertical excitation energies. *Mol. Phys.* **2015**, *113*, 3085-3127.

(10) Dutta, A. K.; Nooijen, M.; Neese, F.; Izsak, R. Exploring the Accuracy of a Low Scaling Similarity Transformed Equation of Motion Method for Vertical Excitation Energies. *J. Chem. Theory Comput.* **2018**, *14*, 72-91.

(11) Helmich-Paris, B. Benchmarks for Electronically Excited States with CASSCF Methods. *J. Chem. Theory Comput.* **2019**, *15*, 4170-4179.

(12) Sarkar, R.; Loos, P. F.; Boggio-Pasqua, M.; Jacquemin, D. Assessing the Performances of CASPT2 and NEVPT2 for Vertical Excitation Energies. *J. Chem. Theory Comput.* **2022**, *18*, 2418-2436.

(13) Loos, P. F.; Scemama, A.; Blondel, A.; Garniron, Y.; Caffarel, M.; Jacquemin, D. A Mountaineering Strategy to Excited States: Highly Accurate Reference Energies and Benchmarks. *J. Chem. Theory Comput.* **2018**, *14*, 4360-4379.

(14) Loos, P. F.; Jacquemin, D. A Mountaineering Strategy to Excited States: Highly Accurate Energies and Benchmarks for Bicyclic Systems. *J. Phys. Chem. A* **2021**, *125*, 10174-10188.

(15) Loos, P. F.; Lipparini, F.; Boggio-Pasqua, M.; Scemama, A.; Jacquemin, D. A Mountaineering Strategy to Excited States: Highly Accurate Energies and Benchmarks for Medium Sized Molecules. *J. Chem. Theory Comput.* **2020**, *16*, 1711-1741.

(16) Loos, P. F.; Scemama, A.; Boggio-Pasqua, M.; Jacquemin, D. Mountaineering Strategy to Excited States: Highly Accurate Energies and Benchmarks for Exotic Molecules and Radicals. *J. Chem. Theory Comput.* **2020**, *16*, 3720-3736.

(17) Loos, P. F.; Lipparini, F.; Matthews, D. A.; Blondel, A.; Jacquemin, D. A Mountaineering Strategy to Excited States: Revising Reference Values with EOM-CC4. *J. Chem. Theory Comput.* **2022**, *18*, 4418–4427.

(18) Kohn, W.; Sham, L. J. Self-consistent equations including exchange and correlation effects. *Phys. Rev.* **1965**, *140*, A1133.

(19) Jacquemin, D.; Perpete, E. A.; Ciofini, I.; Adamo, C.; Valero, R.; Zhao, Y.; Truhlar, D. G. On the Performances of the M06 Family of Density Functionals for Electronic Excitation Energies. *J. Chem. Theory Comput.* **2010**, *6*, 2071-2085.

(20) Peverati, R.; Truhlar, D. G. Performance of the M11 and M11-L density functionals for calculations of electronic excitation energies by adiabatic time-dependent density functional theory. *Phys Chem Chem Phys* **2012**, *14*, 11363-11370.

(21) Isegawa, M.; Peverati, R.; Truhlar, D. G. Performance of recent and high-performance approximate density functionals for time-dependent density functional theory calculations of valence and Rydberg electronic transition energies. *J. Chem. Phys.* **2012**, *137*, 244104.

(22) Jacquemin, D.; Perpete, E. A.; Ciofini, I.; Adamo, C. Assessment of Functionals for TD-DFT Calculations of Singlet-Triplet Transitions. *J. Chem. Theory Comput.* **2010**, *6*, 1532-1537.

(23) Silva, M. R.; Schreiber, M.; Sauer, S. P. A.; Thiel, W. Benchmarks for electronically excited states: Time-dependent density functional theory and density functional theory based multireference configuration interaction. *J. Chem. Phys.* **2008**, *129*, 104103.

(24) Bremond, E.; Savarese, M.; Adamo, C.; Jacquemin, D. Accuracy of TD-DFT Geometries: A Fresh Look. *J. Chem. Theory Comput.* **2018**, *14*, 3715-3727.

(25) Liang, J. S.; Feng, X. T.; Hait, D.; Head-Gordon, M. Revisiting the Performance of Time-Dependent Density Functional Theory for Electronic Excitations: Assessment of 43 Popular and Recently Developed Functionals from Rungs One to Four. *J. Chem. Theory Comput.* **2022**, *18*, 3460-3473.

(26) Hohenberg, P.; Kohn, W. Inhomogeneous electron gas. *Phys. Rev.* **1964**, *136*, B864.

(27) Lu, Y.; Gao, J. Multi-State Density Functional Theory for Ground and Excited States. *ChemRxiv* **2021**, 10.26434/chemrxiv-22021-h26432bmc.

(28) Lu, Y. Y.; Gao, J. L. Multistate Density Functional Theory of Excited States. *J. Phys. Chem. Lett.* **2022**, *13*, 7762-7769.

(29) Lu, Y. Y.; Zhao, R. Q.; Zhang, J.; Liu, M. Y.; Gao, J. L. Minimal Active Space: NOSCF and NOSI in Multistate Density Functional Theory. *J. Chem. Theory Comput.* **2022**, *18*, 6407-6420.

(30) Zhao, R. Q.; Hettich, C. P.; Chen, X.; Gao, J. L. Minimal-active-space multistate density functional theory for excitation energy involving local and charge transfer states. *NPJ Comput. Mater.* **2021**, *7*, 148.

(31) Han, J. T.; Zhao, R. Q.; Guo, Y. J.; Qu, Z. X.; Gao, J. L. Minimal Active Space for Diradicals Using Multistate Density Functional Theory. *Molecules* **2022**, *27*, 3466.

(32) Hettich, C. P.; Zhang, X. Y.; Kemper, D.; Zhao, R. Q.; Zhou, S. Y.; Lu, Y. Y.; Gao, J. L.; Zhang, J.; Liu, M. Y. Multistate Energy Decomposition Analysis of Molecular Excited States. *Jacs Au* **2023**, 10.1021/jacsau.1023c00186.

(33) Cembran, A.; Song, L.; Mo, Y.; Gao, J. Block-localized density functional theory (BLDFT), diabatic coupling, and its use in valence bond theory for representing reactive potential energy surfaces. *J. Chem. Theory Comput.* **2009**, *5*, 2702-2716.

(34) Cohen, A. J.; Mori-Sanchez, P.; Yang, W. T. Challenges for Density Functional Theory. *Chem. Rev.* **2012**, *112*, 289-320.

(35) Levine, B. G.; Ko, C.; Quenneville, J.; Martinez, T. J. Conical intersections and double excitations in time-dependent density functional theory. *Mol. Phys.* **2006**, *104*, 1039-1051.

(36) Theophilou, A. K. Energy Density Functional Formalism for Excited-States. *J Phys C Solid State* **1979**, *12*, 5419-5430.

(37) Gross, E. K. U.; Oliveira, L. N.; Kohn, W. Density-Functional Theory for Ensembles of Fractionally Occupied States .1. Basic Formalism. *Phys. Rev. A* **1988**, *37*, 2809-2820.
(38) Gross, E. K. U.; Oliveira, L. N.; Kohn, W. Rayleigh-Ritz Variational Principle for Ensembles of Fractionally Occupied States. *Phys. Rev. A* **1988**, *37*, 2805-2808.
(39) Lu, Y. Y.; Gao, J. L. Fundamental Variable and Density Representation in Multistate DFT for Excited States. *J. Chem. Theory Comput.* **2022**, *18*, 7403-7411.
(40) Gao, J.; Grofe, A.; Ren, H.; Bao, P. Beyond Kohn–Sham Approximation: Hybrid Multistate Wave Function and Density Functional Theory. *J. Phys. Chem. Lett.* **2016**, *7*, 5143-5149.
(41) Zhao, Y.; Truhlar, D. G. M06 DFT functionals. *Theor. Chem. Acc.* **2008**, *120*, 215.
(42) Perdew, J. P.; Burke, K.; Ernzerhof, M. Generalized gradient approximation made simple. *Phys. Rev. Lett.* **1996**, *77*, 3865-3868.
(43) Ernzerhof, M.; Scuseria, G. E. Assessment of the Perdew-Burke-Ernzerhof exchange-correlation functional. *J. Chem. Phys.* **1999**, *110*, 5029-5036.
(44) Adamo, C.; Barone, V. Toward reliable density functional methods without adjustable parameters: The PBE0 model. *J. Chem. Phys.* **1999**, *110*, 6158-6170.
(45) Zhao, R.; Hettich, C.; Zhang, J.; Liu, M.; Gao, J. Excimer Energies. *J. Phys. Chem. Lett.* **2023**, *14*, 2917-2926.
(46) Zhao, R.; Grofe, A.; Wang, Z.; Bao, P.; Chen, X.; Liu, W.; Gao, J. Dynamic-then-Static Approach for Core Excitations of Open-Shell Molecules. *J. Phys. Chem. Lett.* **2021**, *12*, 7409-7417.
(47) Liu, W.; Hoffmann, M. R. SDS: the 'static-dynamic-static' framework for strongly correlated electrons. *Theor. Chem. Acc.* **2014**, *133*, 1481.
(48) Liu, W. J.; Hoffmann, M. R. iCI: Iterative CI toward Full CI. *J. Chem. Theory Comput.* **2016**, *12*, 1169-1178.
(49) King, H. F.; Staton, R. E.; Kim, H.; Wyatt, R. E.; Parr, R. G. Corresponding orbitals and the nonorthogonality problems in molecular quantum mechanics. *J. Chem. Phys.* **1967**, *47*, 1936-1941.
(50) Mo, Y.; Gao, J. Ab initio QM/MM simulations with a molecular orbital-valence bond (MOVB) method: application to an SN2 reaction in water. *J. Comput. Chem.* **2000**, *21*, 1458-1469.
(51) Mo, Y.; Gao, J. An Ab Initio Molecular Orbital-Valence Bond (MOVB) Method for Simulating Chemical Reactions in Solution. *J. Phys. Chem. A* **2000**, *104*, 3012-3020.

(52) Bao, P.; Hettich, C. P.; Shi, Q.; Gao, J. Block-Localized Excitation for Excimer Complex and Diabatic Coupling. *J. Chem. Theory Comput.* **2021**, *17*, 240-254.
(53) Grofe, A.; Zhao, R.; Wildman, A.; Stetina, T. F.; Li, X.; Bao, P.; Gao, J. Generalization of Block-Localized Wave Function for Constrained Optimization of Excited Determinants. *J. Chem. Theory Comput.* **2021**, *17*, 277-289.
(54) Zhang, J.; Tang, Z.; Zhang, X.; Zhu, H.; Zhao, R.; Lu, Y.; Gao, J. Target State Optimized Density Functional Theory for Electronic Excited and Diabatic States. *J. Chem. Theory Comput.* **2023**, *19*, 1777-1789.
(55) Ziegler, T.; Rauk, A.; Baerends, E. J. Calculation of Multiplet Energies by Hartree-Fock-Slater Method. *Theor. Chim. Acta* **1977**, *43*, 261-271.
(56) Grofe, A.; Chen, X.; Liu, W.; Gao, J. Spin-Multiplet Components and Energy Splittings by Multistate Density Functional Theory. *J. Phys. Chem. Lett.* **2017**, *8*, 4838-4845.
(57) Yang, L. K.; Grofe, A.; Reimers, J.; Gao, J. Multistate density functional theory applied with 3 unpaired electrons in 3 orbitals: The singdoublet and tripdoublet states of the ethylene cation. *Chem. Phys. Lett.* **2019**, *736*, 136803.
(58) Song, L.; Gao, J. On the Construction of Diabatic and Adiabatic Potential Energy Surfaces Based on Ab Initio Valence Bond Theory. *J. Phys. Chem. A* **2008**, *112*, 12925-12935.
(59) Dunning, T. H., Jr. Gaussian basis sets for use in correlated molecular calculations. I. The atoms boron through neon and hydrogen. *J. Chem. Phys.* **1989**, *90*, 1007-1023.
(60) Zhang, J.; Pan, Z.; Zhao, R.; Hou, X.; Zhang, X.; Tang, Z.; Zhang, Y.; Wu, Y.; Liu, W.; Gao, J. *Qbics - Quantum biology, informatics and chemical science.*; Shenzhen Bay Laboratory: Shenzhen, China, 2023.
(61) Schmidt, M. W.; Baldridge, K. K.; Boatz, J. A.; Elbert, S. T.; Gordon, M. S.; Jensen, J. H.; Koseki, S.; Matsunaga, N.; Nguyen, K. A.; Su, S. J.; Windus, T. L.; Dupuis, M.; Montgomery, J. S. *GAMESS*; 1993.
(62) Frisch, M. J.; Trucks, G. W.; Schlegel, H. B.; Scuseria, G. E.; Robb, M. A.; Cheeseman, J. R.; Scalmani, G.; Barone, V.; Petersson, G. A.; Nakatsuji, H.; Li, X.; Caricato, M.; Marenich, A. V.; Bloino, J.; Janesko, B. G.; Gomperts, R.; Mennucci, B.; Hratchian, H. P.; Ortiz, J. V.; Izmaylov, A. F.; Sonnenberg, J. L.; Williams; Ding, F.; Lipparini, F.; Egidi, F.; Goings, J.; Peng, B.; Petrone, A.; Henderson, T.; Ranasinghe, D.; Zakrzewski, V. G.; Gao, J.; Rega, N.; Zheng, G.; Liang, W.; Hada, M.; Ehara, M.; Toyota, K.; Fukuda, R.; Hasegawa, J.; Ishida, M.; Nakajima, T.; Honda, Y.;

Kitao, O.; Nakai, H.; Vreven, T.; Throssell, K.; Montgomery Jr., J. A.; Peralta, J. E.; Ogliaro, F.; Bearpark, M. J.; Heyd, J. J.; Brothers, E. N.; Kudin, K. N.; Staroverov, V. N.; Keith, T. A.; Kobayashi, R.; Normand, J.; Raghavachari, K.; Rendell, A. P.; Burant, J. C.; Iyengar, S. S.; Tomasi, J.; Cossi, M.; Millam, J. M.; Klene, M.; Adamo, C.; Cammi, R.; Ochterski, J. W.; Martin, R. L.; Morokuma, K.; Farkas, O.; Foresman, J. B.; Fox, D. J. *Gaussian 16*; Wallingford, CT, 2016.

(63) Cremer, D.; Filatov, M.; Polo, V.; Kraka, E.; Shaik, S. Implicit and explicit coverage of multi-reference effects by density functional theory. *Int. J. Mol. Sci.* **2002**, *3*, 604-638.

(64) Grafenstein, J.; Cremer, D. Development of a CAS-DFT method covering non-dynamical and dynamical electron correlation in a balanced way. *Molecular Physics* **2005**, *103*, 279-308.

(65) Grafenstein, J.; Cremer, D. The self-interaction error and the description of non-dynamic electron correlation in density functional theory. *Theor. Chem. Acc.* **2009**, *123*, 171-182.

(66) Gunnarsson, O.; Lundqvist, B. I. Exchange and Correlation in Atoms, Molecules, and Solids by Spin-Density Functional Formalism. *Phys. Rev. B* **1976**, *13*, 4274-4298.

(67) Chirgwin, H. B.; Coulson, C. A. The electronic structure of conjugated systems. VI. *Proc. R. Soc. London Ser. A* **1950**, *201*, 196-209.

TOC Graph